

Y. Wang
G. Gioia
A. M. Cuitiño

Department of Mechanical and Aerospace
Engineering,
Rutgers University,
Piscataway, NJ 08854

The Deformation Habits of Compressed Open-Cell Solid Foams

Compressed open-cell solid foams frequently exhibit spatially inhomogeneous distributions of local stretch. The theoretical aspects of this deformation habit have not been clearly elucidated. Here we briefly discuss the energetics of the problem to show that the stretch inhomogeneity stems from the nonconvexity of the underlying potential. We also perform displacement field measurements using the Digital Image Correlation technique, and discuss the results in light of the theory. [S0094-4289(00)01904-6]

1 Introduction

Figures 1(a)-(b) show the microstructure of a typical open-cell solid foam, in this specific case a polyurethane foam. The microstructure is a three-dimensional network of bars of similar length and cross section. In spite of certain irregularities, e.g., Fig. 1(a), we can reasonably imagine the network as if it were composed of repeated basic units, in the form of Fig. 1(c) [1].

Figure 1(d) shows the mechanical response of the foam of Fig. 1(a) subject to uniaxial compressive stretch, λ . The σ - λ curve of Fig. 1(d) is characteristic of compressed open-cell foams (and of some closed-cell foams, too); it is composed of a linear portion, a stress plateau, and a hardening portion [2]. The most interesting feature of this σ - λ curve is the relatively long stress plateau.

The stress plateau of Fig. 1(d) has been associated with the buckling of the network of bars of Fig. 1(b). In fact, a buckling model can be used to predict with good results the length of the plateau and the associated stress. (For a review and extensive references see [2].)

It has been known for some time that the stretch is spatially inhomogeneous in a foam which has been stretched into the stress plateau (see e.g., [3]). In spite of its strengths, the buckling model is not *per se* particularly illuminating of this deformation habit. We have recently suggested that the stretch inhomogeneity may be best elucidated by means of energy considerations [4]. The theoretical aspects of this approach we will expound at length elsewhere (Gioia, Wang and Cuitiño, paper in preparation). The crucial point can be easily grasped, however, by considering the simple model of Fig. 1(c). For a foam stretched along the rise direction we can reduce that model to the two-bar basic unit of Fig. 2(a). Using the reduced model we obtained the strain energy per unit volume of foam (in the original configuration) as a function of the applied stretch. The result is shown in Fig. 2(b).

The strain energy density function $\phi(\lambda)$ of Fig. 2(b) is *nonconvex*. The implications of this fact are momentous [5]. A straightforward nonconvex analysis shows that when the foam is subject to an *overall* applied stretch $\bar{\lambda}$ in the range $\lambda_L > \bar{\lambda} > \lambda_H$, Fig. 3(a), the distribution of local stretch within the specimen is *not* homogeneous and equal to $\bar{\lambda}$ (Gioia, Wang and Cuitiño, paper in preparation). Instead, a volume fraction $0 < \alpha < 1$ of the specimen is subject to a stretch λ_H (the high-density phase) whereas the remaining volume fraction $1 - \alpha$ is subject to a stretch λ_L (the low-density phase), Fig. 3(b). λ_L and λ_H are the *characteristic stretches*, which correspond to two different phases of the microstructure, before and after snap-through buckling, respectively, Figs. 3(c) and (d). The characteristic stretches can be graphically

computed in the form indicated in Fig. 3(a). The value of α follows from compatibility in the form of the law of mixtures

$$\alpha = \frac{\lambda_L - \bar{\lambda}}{\lambda_L - \lambda_H}. \quad (1)$$

The behavior of the foam is fully determined by the function $\bar{\phi}(\lambda)$ (indicated in solid line in Fig. 3(a)), which function is said to effect the *convexification* of $\phi(\lambda)$. Within the plateau range, $\lambda_L > \bar{\lambda} > \lambda_H$, the stress is constant and equal to the plateau stress

$$\sigma_p = - \frac{\phi(\lambda_L) - \phi(\lambda_H)}{\lambda_L - \lambda_H}, \quad (2)$$

see Fig. 3(a). We compare the predicted σ - λ curve with the experimental results in Fig. 4.

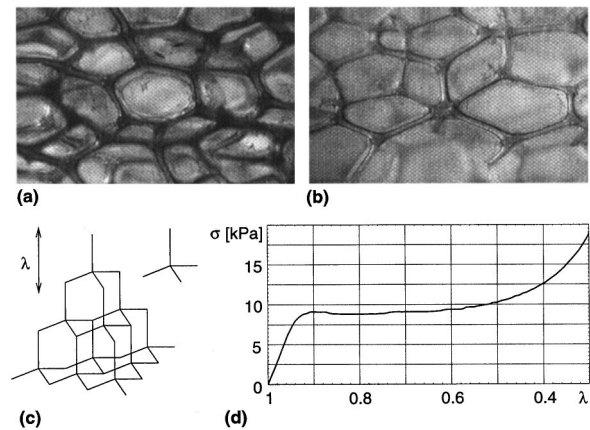


Fig. 1 (a) Microstructure of an open-cell polyurethane solid foam in the vicinity of a pore. (b) This view of the surface of a specimen, where the foam was severed across a plane, reveals the nearly regular microstructure which prevails in most of the foam. (c) Simple model of the microstructure as a regular, three-dimensional network of bars. The four-bar structure in the upper right corner of the figure is the basic unit of the network. The direction indicated in the upper left corner of the figure is the *rise direction* of the foam [1]. (d) Mechanical response of the foam (a-b) subject to uniaxial compressive stretch along the rise direction.

Contributed by the Materials Division for publication in the JOURNAL OF ENGINEERING MATERIALS AND TECHNOLOGY. Manuscript received by the Materials Division January 4, 2000; revised manuscript received April 15, 2000. Guest Editor: Assimina Pelegrini.

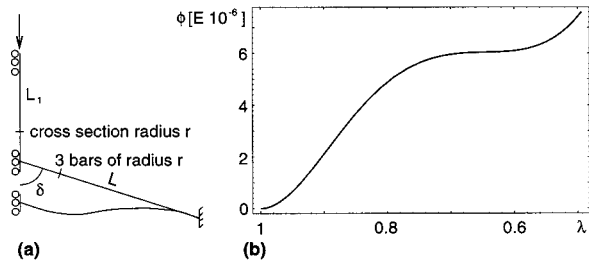


Fig. 2 (a) When the foam is subject to a uniaxial stretch in the rise direction, the four-bar basic unit of Figure 1(c) can be reduced to a two-bar basic unit. The bars are linear elastic of Young's modulus E and circular cross section of radius r ($A = \pi r^2$); they are ruled by Von Kármán's theory of beams. The tilted bar is in actuality three bars, each with the same cross-sectional radius as the vertical bar. (b) Predicted strain energy density of the foam as a function of the applied uniaxial stretch. We have used $L_1/L = 1.5$, $\delta = \cos^{-1}(2/7)$, and the r/L ratio which corresponds to a foam of relative density $\rho_r = 0.01$.

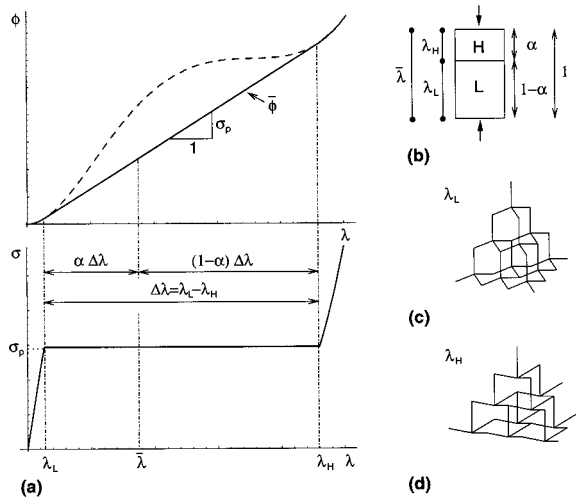


Fig. 3 (a) For an overall applied stretch $\bar{\lambda}$ the total strain energy can be minimized by a straightforward nonconvex analysis. The mechanical response of the foam is governed by $\bar{\phi}(\bar{\lambda})$. Thus the stress for a given $\bar{\lambda}$ is $\sigma = -d\bar{\phi}/d\bar{\lambda}|_{\bar{\lambda}=\bar{\lambda}}$. (b) Inhomogeneous distribution of stretch in the specimen. The high- and low-density phases may not be connected, as shown here, but mixed with each other, see Section 2; the volume fraction α is always given by the compatibility condition, Eq. (1). (c) Microstructure of the low-density phase (before snap-through buckling). (d) Microstructure of the high-density phase (after snap-through buckling).

2 Experiments

In this section, we study experimentally the deformation habits of the foam of Fig. 1. We accomplish this by performing whole-field displacement measurements on the surface of a specimen subject to uniaxial compressive stretch. Due to the extremely low stiffness of the foam, we employ a noncontact measuring method. In addition, since the displacement field is highly irregular at the sub-millimeter level, we opt for a "fuzzy" measuring method capable of averaging the displacement field over a set of windows. The Digital Image Correlation (DIC) technique provides us with the ideal tool. Since its inception in 1982 [6], DIC has been greatly developed [7–10], and found application in a wide variety of problems (see e.g., [11–14]). DIC has recently been employed in foam research [15], where a big-window correlation was adopted. Our aim here is to detect *localized* deformation; conse-

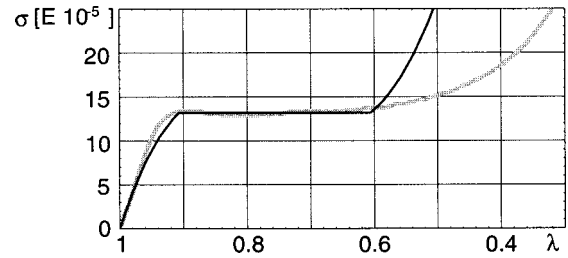


Fig. 4 Experimental (light gray, same curve as in Fig. 1(d)) and predicted stress-stretch curves for the foam of Fig. 1(a)–(b). The predictions are those of the reduced model of Fig. 2(a), properly convexified, with $L_1/L = 1.5$, $\delta = \cos^{-1}(2/7)$, and the r/L ratio which corresponds to a foam of relative density $\rho_r = 0.01$. To fit the curves we have used $E = 68$ MPa and $\rho = 730$ Kgm^{-3} for the bars (the apparent density of the foam is $\rho = 21.9$ Kgm^{-3}); these are reasonable values, within a factor of 2 of the expected ones (perhaps $E = 50$ MPa and $\rho = 1000$ Kgm^{-3} , see [2]). The resulting characteristic stretches are $\lambda_L = 0.91$ and $\lambda_H = 0.60$.

quently, we use a smaller correlation window, namely an array of 15×15 successive pixels, to provide displacement measurements with a standard deviation of 0.1 pixel. This is a compromise between spatial resolution and displacement accuracy.

We used a specimen of height 2.54 cm aligned with the rise direction (axis y) and cross section 10.5×3.72 cm^2 , made of the polyurethane foam of Fig. 1, and compressed it in the direction of the height up to an overall uniaxial stretch $\bar{\lambda} = 0.74$. The speed of the loading plate was $4.2 \cdot 10^{-2}$ cm s^{-1} . We took 11 pictures of the surface of one of the lateral faces of the specimen, at equal intervals of $\bar{\lambda}$, and correlated the successive pictures, one pair at a time, to compute the displacement at the pixels of the reference images. The cumulative displacement of each reference image we transferred to the successive reference image using a bilinear interpolation.

Figure 5(a) is a contour plot of the displacement field $v(x, y)$ in the y direction, on a portion of the face of the specimen. The figure clearly reveals the inhomogeneous nature of the local stretch distribution. The zones of high and low local stretch form roughly parallel strata normal to the y direction; they are most definitely not connected (cf. [3]).

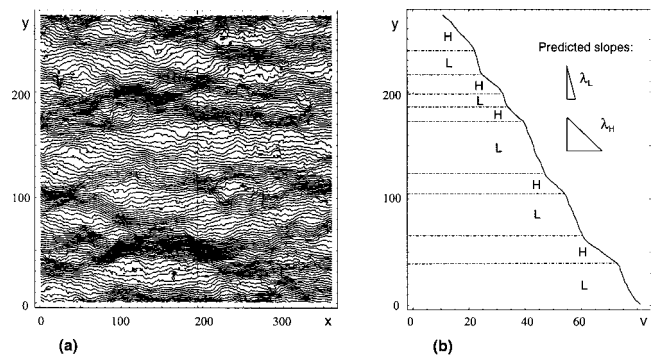


Fig. 5 Displacement field measured by the Digital Image Correlation (DIC) technique. The specimen is subject to an overall stretch in the y direction. v is the displacement along the y direction (y is measured in the original configuration). The units of x , y , and v are pixels. (a) Contour plot of the displacement field $v(x, y)$ on the surface of the specimen. The plot consists of lines of equal v at regular intervals Δv . (b) Plot of the displacement v along the dotted line of (a), and the characteristic slopes which correspond to $\lambda_L = 0.91$ and $\lambda_H = 0.60$ (from Fig. 4).

Figure 5(b) is a plot of the displacement v along the dotted line of Fig. 5(a). The presence of two well-defined slopes is apparent in Fig. 5(b); they represent the low- and high-density phases. In fact, the slope dv/dy is related to the local stretch by the following expression:

$$\frac{dv}{dy} = \lambda - 1. \quad (3)$$

We verify in Fig. 5(b) that the measured slopes compare well with the values computed using Eq. (3) for $\lambda_L = 0.91$ and $\lambda_H = 0.60$, see Fig. 4. From Fig. 5(b) we can also estimate a volume fraction $\alpha = 0.33$. A value of $\bar{\lambda} = 0.76$ is then obtained from Eq. (1), which is in very good agreement with the value of applied stretch, $\bar{\lambda} = 0.74$.

In conclusion, the experimental evidence confirms the inhomogeneous nature of the stretch field in open-cell foams compressed into the stress plateau. This deformation habit stems from the nonconvexity of the underlying energetics. The experiments also provide information beyond the predictive capabilities of the theory. Thus, the experiments indicate that the low- and high-density phases do not arrange themselves into two adjacent regions, but into roughly parallel strata normal to the loading direction.

Acknowledgments

The support from Center for Advanced Food Technology at Rutgers University is gratefully acknowledged.

References

[1] Artavia, L. D., and Macosko, C. W., 1994, "Polyurethane flexible foam formation," *Low Density Cellular Plastics: Physical Basis of Behavior*, Hilyard,

N. C., and Cunningham, A., eds., Chapter 2, pp. 22–55, Chapman & Hall, United Kingdom.

[2] Gibson, L. J., and Ashby, M. F., 1997, *Cellular Solids*, 2nd ed., Cambridge University, United Kingdom.

[3] Fátima Vaz, M., and Fortes, M. A., 1993, "Characterization of deformation bands in the compression of cellular materials," *J. Mater. Sci. Lett.*, **12**, pp. 1408–1410.

[4] Wang, Y., and Cuitiño, A. M., 2000, "Three dimensional modeling of open cell foams with large deformations," *J. Mech. Phys. Solids*, **48**, p. 961.

[5] Ericksen, J. L., 1998, *Introduction to the Thermodynamics of Solids*, 2nd ed., Chapter 3, Springer-Verlag, New York.

[6] Peters, W. H., and Ranson, W. F., 1982, "Digital imaging techniques in experimental stress analysis," *Opt. Eng.*, **21**, pp. 427–431.

[7] Chu, T. C., Ranson, W. F., Sutton, M. A., and Peters, W. H., 1985, "Applications of digital-image-correlation techniques to experimental mechanics," *Exp. Mech.*, **25**, pp. 232–244.

[8] Sutton, M. A., Cheng, M. Q., Peters, W. H., Chao, Y. J., and McNeill, S. R., 1986, "Application of an optimized digital correlation method to planar deformation analysis," *Image Vis. Comput.*, **4**, pp. 143–151.

[9] Bruck, H. A., McNeill, S. R., Sutton, M. A., and Peters, W. H., 1989, "Digital image correlation using Newton-Raphson method of partial differential correction," *Exp. Mech.*, **29**, pp. 261–267.

[10] Vendroux, G., and Knauss, W. G., 1998, "Submicron deformation field measurements: Part 2. Improved digital image correlation," *Exp. Mech.*, **38**, pp. 86–92.

[11] Kahn-Jetter, Z. L., and Chu, T. C., 1990, "Three-dimensional displacement measurements using digital image correlation and photogrammetric analysis," *Exp. Mech.*, **30**, pp. 10–16.

[12] Mizuno, Y., Kawasaki, A., and Watanabe, R., 1995, "In situ measurement of sintering shrinkage in powder compacts by digital image correlation method," *Powder Metall.*, **38**, pp. 191–195.

[13] Tong, W., 1997, "Detection of plastic deformation patterns in a binary aluminum alloy," *Exp. Mech.*, **37**, pp. 452–459.

[14] Cardenas-García, J. F., Yao, H., Zheng, S., and Zartman, R. E., 1998, "Digital image correlation procedure to characterize soil surface layer cracking," *Agron. J.*, **90**, pp. 438–441.

[15] Zhang, D., Zhang, X., and Cheng, G., 1999, "Compression strain measurement by digital speckle correlation," *Exp. Mech.*, **39**, pp. 62–65.